A MODEL FOR THE PREDICTION OF WOUND ROLL DISHING

by

K. A. Cole
Eastman Kodak Company
USA

ABSTRACT

Historically, wound-roll models have been used to predict stress levels which develop within winding and wound rolls. To gain maximum benefit from these models, stresses must be incorporated into defect or failure models. This paper focuses on the development of a wound-roll dishing model. Caliper nonuniformity in both the width and the length direction is incorporated into the model. The effect of some of the important conveyance issues is also included in the model. An experiment is described and the results compared to the analytical predictions. Finally, the model is used to study the effects of process parameters on the level of wound roll dishing.

NOMENCLATURE

c	core diameter, m	s	in-roll radius, m
d	finished roll diameter, m	t	wound-on tension, Kn
D	flexural stiffness, nm	T	in-roll circumferential stress, KPa
E_x	tangent modulus, GPa	u	radial displacement, m
E_y	radial modulus, GPa	v	axial displacement, m
h	web thickness, mm	w	roll width, m
N	in-roll stress resultant, n/cm	δ	axial displacement due to
P	in-roll radial stress, KPa		conveyance effects, m
q	applied axial load, KPa	ε	strain, dimensionless
r	nominal winding radius, m	ϕ	slope, dimensionless
R	radial roll profile, m	υ	Poisson's ratio, dimensionless

Subscripts

d	in-plane radial compression included
M	total number of axial segments
o	initial (from in-plane solution)
p	pressure-roller-assisted winding

Superscripts

^	final minus initial (from out-of-plane solution)
-	in-plane radial compression neglected

INTRODUCTION

Wound rolls are used to package and transport webs from one process to another and ultimately to the end-use customer. The quality of the wound-roll package must be optimized to minimize waste during handling and unwinding in order to insure maximum value to the customer. Wound-roll models have been developed to assist the process engineer with this optimization. Historically, a great deal of effort has been placed on predicting the stresses which develop within the wound roll. However, to gain maximum benefit from these models, stresses must be incorporated into defect or failure models.

One defect mode for which a predictive model has not yet been developed owing to the complexity of the mechanics is the lack of sidewall straightness. Several terms have arisen in the literature to describe this phenomenon. Roisum (1) defines dishing as a nonstraight sidewall formed during winding and telescoping as a nonstraight sidewall formed subsequent to winding (either during handling or unwinding). Frye (2) uses the two terms interchangeably. Alternatively, dishing can be defined as a gradual departure of the sidewall from a straight condition (like a dish) and telescoping as a sudden departure without reference to whether the behavior occurs during or subsequent to winding. For purposes of this paper, we chose this definition. Lack of sidewall straightness can have very significant negative implications in the winding process. Edge damage during handling and lateral misplacement into a downstream operation are two such examples.

Dishing and telescoping are interrelated phenomena and can occur because of several reasons. Lucas (3) presents a very thorough discussion on the mechanical causes of dishing at a double-drum winder used to wind large paper rolls. In his discussion, he states that dishing occurs when axial thrusting forces develop which cause axial movement owing to insufficient mechanical constraint. Thrusting forces arise from any system imbalance such as winder drum misalignment and caliper nonuniformity. Further, if the wound-on tension is not adequate, the thrusting forces can also cause lap-to-lap slippage during winding.

Subsequent to winding, a roll wound with inadequate tension will be prone to further dishing and/or telescoping due to interlayer slippage which can arise from torque transmission failure. A very good discussion of this behavior is given by Bhushan (4).

The thrusting forces which arise during winding due to thickness nonuniformity can cause roll dishing even when no lap-to-lap slippage occurs. This effect is especially important when considering narrow width rolls such as are commonly processed in finishing operations before end-use customer shipment. In these cases, dishing is exacerbated when widthwise thickness nonuniformity which persists in the lengthwise direction. Additionally, for high-aspect-ratio rolls (diameter to width), certain combinations of process conditions can lead to roll instability from column buckling failure of the type described by Timoshenko and Gere (5).

This paper deals with the prediction of wound roll dishing in narrow rolls where no lap-to-lap slippage occurs. A dishing model is presented which predicts the dishing which develops within a winding roll due to the presence of thickness nonuniformity and in-plane or radial stress arising from the wound-on tension stress. The problem is cast into two parts. First, a differential equation and associated boundary conditions are developed which govern the out-of-plane deformations due to the in-plane stress resultants. In this formulation, the roll is assumed to have an initial nonstraight profile. It is then shown that the same set of equations can be used to assess the buckling propensity of the

133

winding roll. This formulation follows a model presented by Benson and Cole (6) which models the deflections within a spinning initially nonflat disk. Next, a model is presented for computing the initial nonstraight profile of the wound roll. Thickness nonuniformity and radial displacements are considered. The in-roll width effects model (7) is used in this formulation. Also considered is the impact of the winding method with regards to how sequential laps are laterally positioned on the winding roll. Numerical methods are then developed to solve for the wound-roll dishing and buckling propensity. A test case is then presented to verify the accuracy of the buckling model followed by experimental dishing results which show good agreement to the theory. Finally, numerical results are obtained for several test cases showing the utility of the model.

PROBLEM FORMULATION

The system of interest is an elastic, orthotropic winding roll with an initial out-of-plane profile caused by axially and radially varying web thickness and in-plane stress. We wish to compute both this initial profile or displacement, v_o, and the final displacement, v, due to the effect of the in-plane stress resultant. Figure 1 and the nomenclature define the variables of the problem. The initial and final displacements of the winding roll are measured relative to a plane perpendicular to the z axis at z=0. The part of the displacement that is due to roll deformation is given by

$$\hat{v} = v - v_o \tag{1}$$

In the derivations which follow, several assumptions are made:

1) in-plane analysis decouples from out-of-plane analysis,
2) initial displacement can be computed from the theoretical model described in (7),
3) generalized plane stress constitutive equations are appropriate,
4) out-of-plane solution is axisymmetric,
5) Kirchoff-Love approximation (8) applies to out-of-plane roll deformations arising from in-plane stress resultants.

In a subsequent section, the model for computation of the initial displacement is presented. In the next section, the differential equation governing the out-of-plane roll deformation due to the in-plane stress resultants is derived.

Out-of-Plane Roll Deformations

The equilibrium equations governing the out-of-plane behavior are found by balancing forces and moments over the elemental section of the roll shown in Figure 2

$$\sum F_z = 0: \qquad r\frac{dQ_r}{dr} + Q_r + rN_r\frac{d\phi}{dr} + N_r\phi + r\frac{dN_r}{dr}\phi = rq \tag{2}$$

$$\sum M_\theta = 0: \qquad M_r + r\frac{dM_r}{dr} - M_\theta + rQ_r = 0 \tag{3}$$

The transverse shear force can be eliminated in equation (2) by means of equation (3) to yield

$$-\frac{2}{r}\frac{dM_r}{dr} - \frac{d^2M_r}{dr^2} + \frac{1}{r}\frac{dM_\theta}{dr} + N_r\frac{d\phi}{dr} + \frac{1}{r}N_r\phi + \frac{dN_r}{dr}\phi = q \qquad (4)$$

Next, consider the orthotropic constitutive relationships

$$\hat{\varepsilon}_\theta = \frac{\hat{T}}{E_x} + \frac{\upsilon_{\theta r}\hat{P}}{E_y}, \qquad \hat{\varepsilon}_r = -\frac{\hat{P}}{E_y} - \frac{\upsilon_{r\theta}\hat{T}}{E_x} \qquad (5)\,(6)$$

where the strain-displacement relationships are given by

$$\hat{\varepsilon}_\theta = \frac{\hat{u}}{r}, \qquad \hat{\varepsilon}_r = \frac{d\hat{u}}{dr} \qquad (7)\,(8)$$

Equations (5) and (6) can be inverted to yield

$$\hat{P} = \frac{E_xE_y\{\hat{\varepsilon}_r + \upsilon\hat{\varepsilon}_\theta\}}{\upsilon^2E_y - E_x}, \qquad \hat{T} = -\frac{E_xE_y\left\{\upsilon\hat{\varepsilon}_r + \dfrac{E_x}{E_y}\hat{\varepsilon}_\theta\right\}}{\upsilon^2E_y - E_x} \qquad (9)\,(10)$$

where use is made of the following derived from strain energy considerations (9)

$$\frac{\upsilon_{\theta r}}{E_y} = \frac{\upsilon_{r\theta}}{E_x} = \frac{\upsilon}{E_x} \qquad (11)$$

To proceed, forces and moments acting on the middle surface must be obtained using the stress resultants which are found by integrating the stresses acting on the side faces of the roll elemental section of Figure 2

$$N_r = \int_{-w/2}^{w/2} P_o\,dz, \quad M_r = -\int_{-w/2}^{w/2} \hat{P}z\,dz, \quad M_\theta = \int_{-w/2}^{w/2} \hat{T}z\,dz \qquad (12)\,(13)\,(14)$$

Equations (9) and (10) can now be substituted into equations (13) and (14) using equations (7) and (8) and the Kirchoff-Love approximation (8)

$$\hat{u} = -z\frac{d\hat{v}}{dr} \qquad (15)$$

to obtain expressions for the moments in terms of the roll deformation

$$M_r = -D\left\{\frac{d^2\hat{v}}{dr^2} + \upsilon\frac{1}{r}\frac{d\hat{v}}{dr}\right\}, \qquad M_\theta = -D\left\{\upsilon\frac{d^2\hat{v}}{dr^2} + g^2\frac{1}{r}\frac{d\hat{v}}{dr}\right\} \qquad (16)\,(17)$$

where

135

$$g \equiv \sqrt{\frac{E_x}{E_y}} = \text{modulus ratio} \tag{18}$$

$$D \equiv \frac{g^2 E_y}{g^2 - v^2} \frac{w^3}{12} \approx \frac{E_y w^3}{12} \text{ for } g^2 >> v^2 \text{which is true for wound rolls} \tag{19}$$

The governing differential equation for out-of-plane deformation is finally found by substitution of equations (16) and (17) into equation (4) along with $\phi = \frac{dv}{dr}$

$$D\left\{ \frac{d^4\hat{v}}{dr^4} + \frac{2}{r}\frac{d^3\hat{v}}{dr^3} - \frac{g^2}{r^2}\frac{d^2\hat{v}}{dr^2} + \frac{g^2}{r^3}\frac{d\hat{v}}{dr} \right\} + N_r \frac{d^2 v}{dr^2} + \left\{ \frac{1}{r}N_r + \frac{dN_r}{dr} \right\}\frac{dv}{dr} = q \tag{20}$$

Associated with this ordinary differential equation are four boundary conditions. At the core, the displacement and slope of the roll are given by

$$\hat{v}\left(r = \frac{c}{2} \right) = 0, \quad \frac{d\hat{v}}{dr}\left(r = \frac{c}{2} \right) = 0 \tag{21} \tag{22}$$

while at the roll periphery, conditions representing a free outer edge are expressed as

$$\left\{ \frac{d^2\hat{v}}{dr^2} + \frac{v}{r}\frac{d\hat{v}}{dr} \right\}\bigg|_{r=\frac{d}{2}} = 0, \quad \left\{ \frac{d^3\hat{v}}{dr^3} + \frac{1}{r}\frac{d^2\hat{v}}{dr^2} - \frac{g^2}{r^2}\frac{d\hat{v}}{dr} \right\}\bigg|_{r=\frac{d}{2}} = 0 \tag{23} \tag{24}$$

Equation (20) subject to equations (21) through (24) provides the means to find the out-of-plane axisymmetric deformation of a winding roll due to the in-plane stress resultant arising from winding tension acting in concert with an initial out-of-plane profile caused by thickness nonuniformity. Additionally, displacements caused by an externally applied axisymmetric axial load are also included. If this force is set to zero, equation (20) can be rewritten using equation (1) as

$$L[\hat{v}(r)] = D\left\{ \frac{d^4\hat{v}}{dr^4} + \frac{2}{r}\frac{d^3\hat{v}}{dr^3} - \frac{g^2}{r^2}\frac{d^2\hat{v}}{dr^2} + \frac{g^2}{r^3}\frac{d\hat{v}}{dr} \right\} + N_r \frac{d^2\hat{v}}{dr^2} + \left\{ \frac{1}{r}N_r + \frac{dN_r}{dr} \right\}\frac{d\hat{v}}{dr}$$

$$= -N_r \frac{d^2 v_o}{dr^2} - \left\{ \frac{1}{r}N_r + \frac{dN_r}{dr} \right\}\frac{dv_o}{dr} \tag{25}$$

The system of equations (21) through (25) is now formally equivalent to a winding roll with a straight initial profile. As such, they can be used for two distinct purposes. First, the equations can be solved directly to yield the out-of-plane displacements due to the in-plane stress resultants. To perform this analysis, the initial out-of-plane profile must first be computed as outlined in the next section.

A second use of this system of equations is to evaluate conditions under which axial buckling occurs. For this purpose, the right hand side of equation (25) is replaced with $\lambda_m E_m(r)$ and conditions found for which nontrivial solutions exist for $\lambda_m = 0$. Here

136

λ_m denotes an eigenvalue and m denotes the number of nodal circles or crossings of the $z = 0$ plane in the associated eigenvector, $E_m(r)$. The lowest buckling mode will occur for $m = 0$ since we are dealing with an axisymmetric problem. We will return to this after describing the method for the computation of the initial profile.

Initial Out-of-Plane Profile

To compute the initial out-of-plane profile or displacement due to in-plane stresses, we first consider the case shown in Figure 3. Here, for illustrative purposes, the web is assumed to have a trapezoidal thickness distribution

$$h(r,z) = h_n(r) - \phi_n(r)z \tag{26}$$

where $h_n(r)$ is the mean thickness and $\phi_n(r)$ is the axial slope or taper of the web. If the web is now wound into a roll, an expression for the radially dependent slope within the roll can be written as

$$\bar{\phi}_o(s) = \int_{c/2}^{s} \frac{\phi_n(s')}{h_n(s')} ds', \qquad c/2 \le s \le r \le d/2 \tag{27}$$

where the bar indicates that radial compression is neglected. The out-of-plane profile can be determined from equation (27) if it is assumed that each individual lap is axially aligned to the preceding lap as it is added to the roll

$$\bar{v}_o(s) = \int_{c/2}^{s} \bar{\phi}_o(s') ds' = \int_{c/2}^{s}\int_{c/2}^{s'} \frac{\phi_n(s'')}{h_n(s'')} ds'' \, ds', \qquad c/2 \le s \le r \le d/2 \tag{28}$$

In practice, the web thickness distribution will be more complex than that given by equation (26). Further, in-roll compression will modify the distribution of the slope within the roll. Lastly, the assumption that the laps are axially aligned will depend on how the roll is wound.

The first two effects are accommodated by the in-roll width effects model (7). In this model, the radial profile at the periphery of the winding roll, $R_d(s,z)$, is predicted as is the compression at this radial location due to the addition of subsequent laps, $u_o(s,z)$. We can thus write an expression for the radial roll profile within the roll during winding as

$$R_{dr}(s,z) = R_d(s,z) + u_o(s,z), \qquad c/2 \le s \le r \le d/2 \tag{29}$$

The means used to obtain this solution is to first partition the web into a discrete number of axial segments. Within each of these segments, the process parameters as well as the stresses and radial displacements are width independent. Therefore, the more physically realistic case of a general axial and radial thickness nonuniformity can be handled.

137

Coupling between the segments is achieved via the outer-lap analysis which is based on equilibrium considerations. This analysis is used to partition the winding tension between segments and makes use of the widthwise distribution of radius at the periphery of the winding roll, the total winding tension within the winding lap, and the radial stiffness of each segment which is computed, as are the subsequent incremental stresses and displacements, using Hakiel's model (10).

Due to the partitioning of the winding roll, a discrete set of ordered pairs are computed which describe the radial roll profile within the roll during winding

$$(z_1, R_{dr1}), (z_2, R_{dr2}), \dots, (z_M, R_{drM})$$ (30)

From these ordered pairs, we are able to compute using the method of least squares the slope within the roll

$$R_{dr}^{fit}(s,z) = a_o(s) + a_1(s)z = a_o(s) + \phi_o(s)z$$ (31)

where the coefficients are selected to yield a "best possible fit" to the actual profile. In this case, the "best" system is the one which renders the sum of the squares of the deviations, $\sum_{i=1}^{M} \left[R_{dr}^{fit}(s, z_i) - R_{dri} \right]^2$ a minimum.

We now use equation (28) to compute the initial profile of the winding roll

$$v_o(s) = \int_{c/2}^{s} \phi_o(s')ds', \qquad c/2 \le s \le r \le d/2$$ (32)

Equation (32) assumes axial alignment between successive laps during winding. In practice, the method of winding will impact this and perfect alignment between the laps will not occur. This effect must be computed if we are to successfully model the final displacement which occurs within the winding roll.

In this paper, we consider the case of pressure-roller winding where an idling roller with a compliant covering is added to the periphery of the winding roll. This method is typically employed to improve winding reliability and to enable high speed winding. If the web wraps the pressure roller, then two subcases present themselves. First, if flanges are used on the pressure roller, then no lap-to-lap offsets will arise and the expression given by equation (32) will be correct. However, in this case, axial constraint in the pressure roller and winding roll will result in an overconstrained system since the roll seeks to develop an initial out-of-plane profile. Under extreme conditions, rolls wound in this way have the potential to exhibit sudden axial shifts when the forces within the roll are not sufficient to balance the applied forces which develop due to overconstraint.

This leads to the second subcase where the pressure roller is not flanged. Typically, in this application, the pressure roller is rigidly mounted with provision made to insure that the lateral position of the web onto the pressure roller is always at the same axial

position. Thus, a component of tracking will arise which will always cancel the developing initial offset of the periphery of the winding roll

$$\delta_p(r) = -v_o(r) \tag{33}$$

The variable r in equation (33) indicates that evaluation of this component within the winding roll is to occur using the slope of the roll when the periphery is at the point of interest. For this case, the initial profile of the winding roll is found by adding equation (33) to equation (32). As will be shown, experiments indicate this to be a very reasonable predictor of lap-to-lap offset. Further, from the standpoint of winding reliability, this method is preferred in that excessive applied constraint forces do not develop.

NUMERICAL SOLUTION

The solution for the initial out-of-plane profile is obtained by adding a least-squares algorithm to the in-roll width effects model according to equation (31). The initial profile neglecting lap-to-lap offsets is found by employing Simpson's rule to perform the numerical integration indicated by equation (32). The effect of lap-to-lap offsets due to the presence of a rigidly mounted, unflanged pressure roller is predicted in the same fashion.

We now turn our attention to the numerical solution of equation (25) governing the axial displacements within the initially displaced winding roll due to the in-plane stress resultants. The radial domain is divided into N equal-sized steps

$$\Delta = \frac{d-c}{2N} \tag{35}$$

with node points located at

$$r^n = \frac{c}{2} + n\Delta \tag{36}$$

A superscript indicates a function evaluated at the corresponding node point, for example

$$\hat{v}^n = \hat{v}\left(r^n\right), \text{ etc.} \tag{37}$$

Derivatives in $\hat{v}$ are approximated by the following central, finite difference formulas

$$\frac{d\hat{v}^n}{dr} = \frac{-\hat{v}^{n+2} + 8\hat{v}^{n+1} - 8\hat{v}^{n-1} + \hat{v}^{n-2}}{12\Delta} \tag{38}$$

$$\frac{d^2\hat{v}^n}{dr^2} = \frac{-\hat{v}^{n+2} + 16\hat{v}^{n+1} - 30\hat{v}^n + 16\hat{v}^{n-1} - \hat{v}^{n-2}}{12\Delta^2} \tag{39}$$

$$\frac{d^3\hat{v}^n}{dr^3} = \frac{\hat{v}^{n+2} - 2\hat{v}^{n+1} + 2\hat{v}^{n-1} - \hat{v}^{n-2}}{2\Delta^3} \tag{40}$$

139

$$\frac{d^4\hat{v}^n}{dr^4} = \frac{\hat{v}^{n+2} - 4\hat{v}^{n+1} + 6\hat{v}^n - 4\hat{v}^{n-1} + \hat{v}^{n-2}}{\Delta^4} \tag{41}$$

Similar expressions can be written for the derivatives of N_r and v_o. Substituting equations (35) through (41) into equation (25) provides $N+1$ equations in $N+5$ unknowns

$$R^n\hat{v}^{n-2} + S^n\hat{v}^{n-1} + T^n\hat{v}^n + U^n\hat{v}^{n+1} + V^n\hat{v}^{n+2} = F^n \tag{42}$$

where $n = 0,1,2,\ldots,N$ and

$$R^n = D^n\left\{\frac{1}{\Delta^4} - \frac{1}{r^n\Delta^3} + \frac{g^2}{12r^{n2}\Delta^2} + \frac{g^2}{12r^{n3}\Delta}\right\} - N_r^n\frac{1}{12\Delta^2} + \left\{\frac{1}{r^n}N_r^n + \frac{dN_r^n}{dr}\right\}\frac{1}{12\Delta} \tag{43}$$

$$S^n = D^n\left\{\frac{-4}{\Delta^4} + \frac{2}{r^n\Delta^3} - \frac{4g^2}{3r^{n2}\Delta^2} - \frac{2g^2}{3r^{n3}\Delta}\right\} + N_r^n\frac{4}{3\Delta^2} - \left\{\frac{1}{r^n}N_r^n + \frac{dN_r^n}{dr}\right\}\frac{2}{3\Delta} \tag{44}$$

$$T^n = D^n\left\{\frac{6}{\Delta^4} + \frac{5g^2}{2r^{n2}\Delta^2}\right\} - N_r^n\frac{5}{2\Delta^2} \tag{45}$$

$$U^n = D^n\left\{\frac{-4}{\Delta^4} - \frac{2}{r^n\Delta^3} - \frac{4g^2}{3r^{n2}\Delta^2} + \frac{2g^2}{3r^{n3}\Delta}\right\} + N_r^n\frac{4}{3\Delta^2} + \left\{\frac{1}{r^n}N_r^n + \frac{dN_r^n}{dr}\right\}\frac{2}{3\Delta} \tag{46}$$

$$V^n = D^n\left\{\frac{1}{\Delta^4} + \frac{1}{r^n\Delta^3} + \frac{g^2}{12r^{n2}\Delta^2} - \frac{g^2}{12r^{n3}\Delta}\right\} - N_r^n\frac{1}{12\Delta^2} - \left\{\frac{1}{r^n}N_r^n + \frac{dN_r^n}{dr}\right\}\frac{1}{12\Delta} \tag{47}$$

Since the initial displacement, v_o, is known, the right hand side can be written in a similar fashion. However, since boundary conditions do not exist for these displacements, forward and backward differences must be resorted to at the roll boundaries. Thus, for $n = 2,3,\ldots,N-2$

$$F^n = -N_r^n\left\{\frac{-v_o^{n+2} + 16v_o^{n+1} - 30v_o^n + 16v_o^{n-1} - v_o^{n-2}}{12\Delta^2}\right\}$$

$$-\left\{\frac{1}{r^n}N_r^n + \frac{dN_r^n}{dr}\right\}\left\{\frac{-v_o^{n+2} + 8v_o^{n+1} - 8v_o^{n-1} + v_o^{n-2}}{12\Delta}\right\} \tag{48}$$

and for $n = 0,1$

$$F^n = -N_r^n \left\{ \frac{-v_o^{n+3} + 4v_o^{n+2} - 5v_o^{n+1} + 2v_o^n}{\Delta^2} \right\}$$

$$-\left\{ \frac{1}{r^n} N_r^n + \frac{dN_r^n}{dr} \right\} \left\{ \frac{2v_o^{n+3} - 9v_o^{n+2} + 18v_o^{n+1} - 11v_o^n}{6\Delta} \right\} \tag{49}$$

and for $n = N - 1, N$

$$F^n = -N_r^n \left\{ \frac{2v_o^n - 5v_o^{n-1} + 4v_o^{n-2} - v_o^{n-3}}{\Delta^2} \right\}$$

$$-\left\{ \frac{1}{r^n} N_r^n + \frac{dN_r^n}{dr} \right\} \left\{ \frac{11v_o^n - 18v_o^{n-1} + 9v_o^{n-2} - 2v_o^{n-3}}{6\Delta} \right\} \tag{50}$$

The radial derivative of the stress resultant is likewise found for $n = 2, 3, \ldots, N - 2$

$$\frac{dN_r^n}{dr} = \frac{-N_r^{n+2} + 8N_r^{n+1} - 8N_r^{n-1} + N_r^{n-2}}{12\Delta} \tag{51}$$

and for $n = 0, 1$

$$\frac{dN_r^n}{dr} = \frac{2N_r^{n+3} - 9N_r^{n+2} + 18N_r^{n+1} - 11N_r^n}{6\Delta} \tag{52}$$

and for $n = N - 1, N$

$$\frac{dN_r^n}{dr} = \frac{11N_r^n - 18N_r^{n-1} + 9N_r^{n-2} - 2N_r^{n-3}}{6\Delta} \tag{53}$$

The boundary conditions supply the remaining four equations needed to complete the system. Substituting equations (35) to (41) into equations (21) to (24) gives

$$\hat{v}^o = 0, \qquad \hat{v}^{-2} - 8\hat{v}^{-1} + 8\hat{v}^1 - \hat{v}^2 = 0 \tag{54} \tag{55}$$

$$\left\{ -\frac{1}{12\Delta} + \frac{v}{6d} \right\} \hat{v}^{N-2} + \left\{ \frac{4}{3\Delta} - \frac{4v}{3d} \right\} \hat{v}^{N-1} + \left\{ -\frac{5}{2\Delta} \right\} \hat{v}^N$$

$$+\left\{ \frac{4}{3\Delta} + \frac{4v}{3d} \right\} \hat{v}^{N+1} + \left\{ -\frac{1}{12\Delta} - \frac{v}{6d} \right\} \hat{v}^{N+2} = 0 \tag{56}$$

141

$$\left\{-\frac{1}{2\Delta^2}-\frac{1}{6d\Delta}-\frac{g^2}{3d^2}\right\}\hat{v}^{N-2}+\left\{\frac{1}{\Delta^2}+\frac{8}{3d\Delta}+\frac{8g^2}{3d^2}\right\}\hat{v}^{N-1}+\left\{-\frac{5}{d\Delta}\right\}\hat{v}^{N}$$

$$+\left\{-\frac{1}{\Delta^2}+\frac{8}{3d\Delta}-\frac{8g^2}{3d^2}\right\}\hat{v}^{N+1}+\left\{\frac{1}{2\Delta^2}-\frac{1}{6d\Delta}+\frac{g^2}{3d^2}\right\}\hat{v}^{N+2}=0 \tag{57}$$

In the process of solution, values for $\hat{v}^n, n = -2, -1, N+1$ and $N+2$ will be computed. They have no physical meaning.

Lastly, we consider the solution to the radial buckling problem posed by equation (25)

$$L\left[E_m(r)\right] = \lambda_m E_m(r) \tag{58}$$

The boundary conditions are the same as equations (21) through (24) with $E_m(r)$ replacing $\hat{v}$. Here, we wish to find the discrete values of λ_m which yield nontrivial solutions for $E_m(r)$. More to the point, we would like to evaluate conditions under which the lowest eigenvalue becomes equal to zero. In this case, the winding roll will be radially unstable and axial buckling will occur.

To find the lowest eigenvalue, we use the method of Barasch and Chen (11). The method, in brief, consists of the following steps. A value of λ is chosen and two displacement functions are generated. The first has boundary values

$$E = \frac{dE}{dr} = \frac{d^3E}{dr^3} = 0, \quad \frac{d^2E}{dr^2} = 1 \text{ at } r = \frac{c}{2} \tag{59}$$

and the second has boundary values

$$E = \frac{dE}{dr} = \frac{d^2E}{dr^2} = 0, \quad \frac{d^3E}{dr^3} = 1 \text{ at } r = \frac{c}{2} \tag{60}$$

Equation (58) generates subsequent values on $\frac{c}{2} \leq r \leq \frac{d}{2}$. The requirements $E = 0$ and $\frac{dE}{dr} = 0$ at $r = \frac{c}{2}$ follow from the inner boundary conditions. The choices for $\frac{d^2E}{dr^2}$ and $\frac{d^3E}{dr^3}$ are nonphysical, but will lead to nontrivial displacement functions. The question is whether a linear combination of these can satisfy the free-edge boundary conditions. Only for discrete values, $\lambda = \lambda_m$, will this be possible. We use standard matrix techniques and a Newton/Raphson iteration to find the lowest eigenvalue.

RESULTS

Case 1 - Buckling of a Plate

A test case with published analytical results was selected to verify the implemented numerical solution to the buckling problem. Results are given in (5) for the lowest

critical buckling force symmetrically distributed around a circular plate with a hole at the center and both clamped and simply supported boundary conditions at the perimeter. The boundary conditions in the model were modified to simulate these conditions. The method of solution was to first solve the in-roll problem to obtain the distributed in-roll stress resultant and subsequently compute the lowest eigenvalue from the buckling analysis. Iteration on wound-on tension continues until the eigenvalue becomes zero. The inputs to the model are shown in Table 1a. As can be seen, seven different geometries were evaluated (core/finish diameter ratio from 0.05 to 0.35). The core stiffness was selected to be nearly zero to approximate the force free center and the winding tension was manually inputed such that the tension was nearly zero except in the last lap which approximates the applied forces of the problem.

Results for both the clamped and simply supported conditions are given in Table 1b. Comparison in terms of the winding tension in the outer lap is made between the analytical and numerical results. As can be seen, the agreement between the two is very good with the maximum deviation equal to 3.1%. It is interesting to note that the model successfully predicts the local minimum seen in the clamped case at the core/finish diameter ratio of 0.20. From these results, we conclude that the model is accurate and capable of predicting axial buckling.

Case 2 - Experimental Verification

As a second case, winding experiments with an unflanged pressure roller were performed on 35 mm wide polyethylene terephthalate support. Two rolls, each 1800 m in length, were spliced together to form one roll. The rolls were selected based on the presence of significant thickness nonuniformity. The experiment consisted of winding the roll five times at one tension and nip force level onto a phenolic core and subsequently measuring the dishing profile after winding. The dish was measured at four angular positions (every 90°) by means of a dial indicator mounted to a straightedge referenced to the end of the core. It was found that averaging the angular data eliminated variability which arose due to lack of perpendicularity between the end of the core and the rotation axis. The conditions of the experiment, shown in Table 2, were then inputted to the numerical model. Thickness nonuniformity is shown in Figure 4. These results were obtained by taking the average of three LVDT traces measured every 300 m. As can be seen, the nonuniformity is very persistent.

Experimental and analytical results are shown in Figure 5. The solid curves represent the model results for both cases of pressure roller winding. The experimental data with 95% confidence limits are also shown. As can be seen, the unflanged pressure roller model results agree very well with the experimental data. The perimeter of the roll is axially very well aligned with the axial position of the web near the core. It is further seen that the additional deflection from out-of-plane deformation of the roll due to the distributed in-roll stress resultant is quite small. Also shown is the lowest eigenvalue which is substantially positive as expected indicating minimal likelihood of axial buckling.

Case 3 - Process Study

Using the conditions of the previous case, the effect of two levels of width and three levels of thickness nonuniformity on initial displacement and maximum roll deformation were studied with the model. In addition, the lowest eigenvalue was computed. Results are shown in Table 3. It is seen that when the support is 35 mm in width, the

deformation of the roll due to the in-roll stress resultant is small relative to the initial displacement while for the narrower roll, the magnitude of the roll deformation becomes more significant. At the same time, the lowest eigenvalue is significantly lower and approaching zero which implies that the roll is becoming much more prone to axial buckling. Finally, the effect of thickness nonuniformity is seen to be more significant for the narrower width support as evidenced by the comparison between the last case of the 35 mm support and the second case of the 16 mm support. The initial displacement is larger for the narrower web because less in-roll compression occurs thereby resulting in less mitigation of the stacking effect of the trapezoidal shaped laps.

SUMMARY

A wound-roll dishing model has been presented. Caliper nonuniformity in both the width and the length direction has been incorporated into the model. The effect of some of the important conveyance issues was also included in the model. The model was correlated to closed-form analytical solutions as well as to experimental results. Finally, the model was used to study the effect of thickness nonuniformity and web width on the level of wound roll dishing and the propensity for axial buckling.

ACKNOWLEDGMENTS

REFERENCES

1. Roisum, D.R., The Mechanics of Winding, TAPPI Press, Atlanta, Georgia, 1990, pg. 109.

2. Frye, K.G., Winding, TAPPI Press, Atlanta, Georgia, 1990, pg. 106.

3. Lucas, R.G., "Dishing in Winding Rolls of Paper", TAPPI Journal, Vol. 60, No. 7, July 1977, pp. 121-125.

4. Bhushan, B., Hahn, F.W., Sharma, B.S., and Connolly, D., "Long-Term Reliability of Magnetic Tapes For Digitial Recording", Tribology and Mechanics of Magnetic Storage, ASLE SP-16, Oct. 1984, pp. 132-147.

5. Timoshenko, S.P. and Gere, J.M., Theory of Elastic Stability, McGraw-Hill Book Company, New York, 2nd ed., 1961, pp. 389-392.

6. Benson, R.C. and Cole, K.A., "Transverse Runout of a Nonflat Spinning Disk", Tribology and Mechanics of Magnetic Storage, ASLE SP-29, Oct. 1990, pp. 1-8.

7. Cole, K.A and Hakiel, Z., "A Nonlinear Wound Roll Stress Model Accounting for Widthwise Web Thickness Nonuniformities", Symposium on Web Handling, AMD-Vol 149, Nov. 1992, pp. 13-24.

8. Flugge, W., Stresses in Shells, Springer-Verlag, Berlin, 1960.

9. McCullough, R.L., "Anisotropic Elastic Behavior of Crystalline Polymers", Treatise on Material Science and Technology, Vol. 10, Part-B, 1977, pg. 463.

10. Hakiel, Z., "Nonlinear Model for Wound Roll Stresses", TAPPI Journal, Vol. 70, No. 5, May 1987, pp. 113-117.

11. Barasch, S. and Chen, Y., "On the Vibration of a Rotating Disk", ASME Journal of Applied Mechanics, Vol. 39, No. 4, Dec. 1972, pp. 1143-1144.
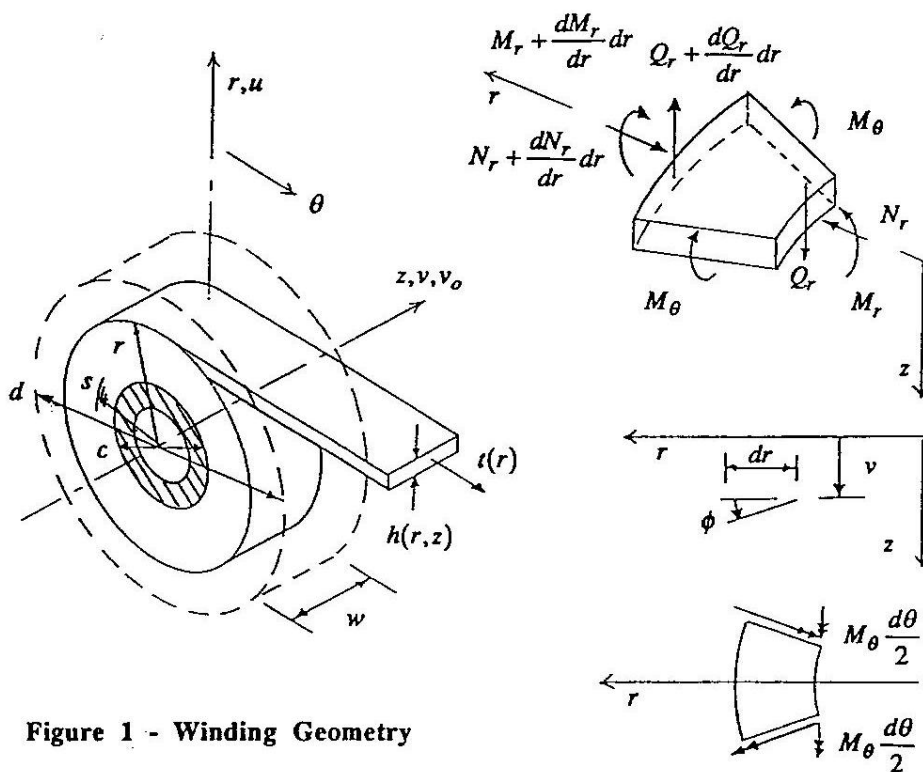
Figure 1 - Winding Geometry

Figure 2 - Roll Elemental Section
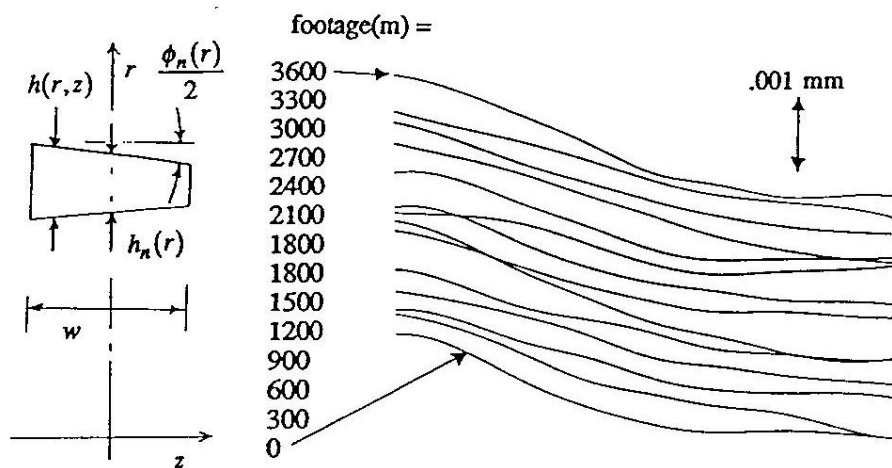(Out-of-Plane Deformations)

Figure 3 - Idealized
Thickness Nonumiformity

Figure 4 - Thickness Nonuniformity,
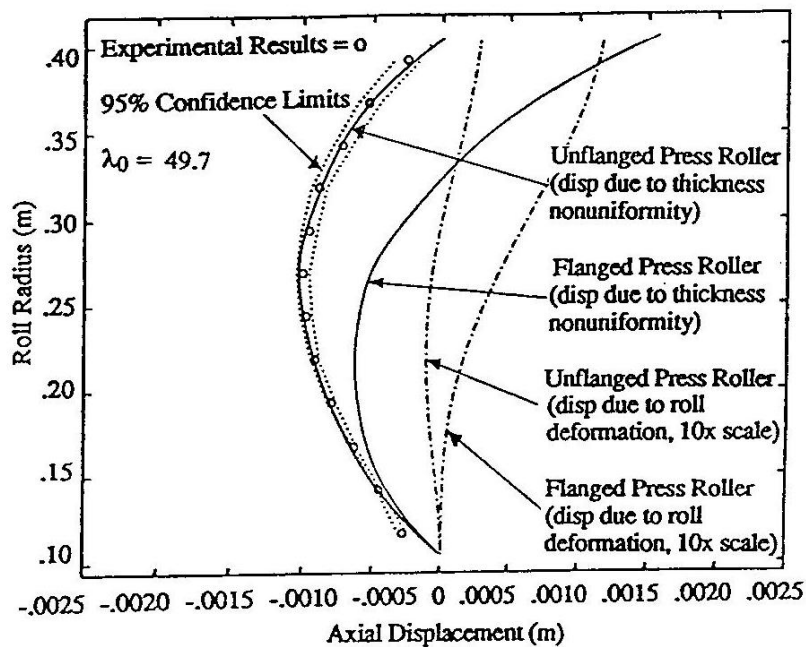Experimental Test Case

145

Figure 5 - Axial Displacement Vs Roll Radius
Experiment Vs Model

c (m)	0.0635, .1270, .1905, .2540, .3175, .3810, .4445		
h (mm)	12.1, 11.4, 10.8, 10.2, 9.53, 8.89, 8.26		
d (m)	1.27		
w(m)	0.0160	core stiffness (Pa)	0.690
E_x, E_y(GPa)	4.69	number of laps	100
v	0.333		

Table 1a - Case 1 Model Inputs

Critical Winding Tension (Kn)
(Outer Lap Only)

c/d	Ref (5) Fig 31b	Model (Clamped)	% Diff	Ref(5) Fig 31a	Model (SS)	% Diff
0.05	20.27	19.97	-1.5	5.812	5.991	3.1
0.10	19.70	19.21	-2.5	5.672	5.744	1.3
0.15	19.14	18.66	-2.5	5.386	5.411	0.46
0.20	18.85	18.62	-1.2	5.103	5.066	-0.73
0.25	19.42	19.19	-1.2	4.820	4.716	-2.2
0.30	20.84	20.42	-2.0	4.537	4.408	-2.8
0.35	22.68	22.40	-1.2	4.254	4.139	-2.7

Table 1b - Case 1 Model Results

146

material	polyethylene terephthalate (PET)	E_y(GPa) / P(KPa)	Look up table: E_y(GPa)
c(m)	0.22	0.0	2.94e-3
d(m)	0.83	13.8	5.26e-3
h_{mean}(mm)	0.1362	27.6	1.31e-2
w(m)	0.0350	41.4	1.84e-2
core stiffness(GPa)	0.462	138	6.80e-2
E_x(GPa)	4.69	345	1.84e-1
friction (kinetic)	0.26	690	4.17e-1
t(Kn)	0.0193	1380	8.26e-1
wind tens, nip force(Kn)	0.00890, 0.0400	5520	2.85e0
v	0.01	9660	3.01e0
M	9	number of laps	2237

Table 2 - Model Inputs, Experimental Test Case

Width (m)	Thickness Nonuniformity (mm/35mm)	Maximum Initial Displacement (m)	Maximum Roll Deformation (m)	λ_o
0.035	0.0	0.0	0.0	48.8
0.035	0.00127	-0.724e-3	0.0185e-3	49.2
0.035	0.00254	-1.25e-3	0.0378e-3	50.3
0.016	0.0	0.0	0.0	3.75
0.016	0.00254	-1.58e-3	0.257e-3	3.72
0.016	0.00508	-2.62e-3	0.532e-3	3.69

Table 3 - Dishing and Buckling Process Study Case

Question - When I think of 35mm wide web at Kodak, I think of perforated film, how does it affect roll behavior, is it helpful or is it more of an hindrance?

Answer - What we studied here was not perforated, perforations can add an effect because the radial modulus is different in the non-perforated area. I haven't studied this but I would say that it would cause the roll to be less prone to buckling. Perforated areas tend to be stiffer than non-perforated areas of the web.

Question - Early we heard a talk from DuPont, they mentioned cases where master rolls could be wound of flat film and I've had an opportunity to work with DuPont film with knurled edge film. How does that relate to telescoping and how layers wind on one another?

Answer - This model provides a starting point as to what would happen to a knurled master roll from the standpoint of axial stability. The model we presented in 1992 is capable of handling thickness nonuniformity due to knurling. We would like to extend todays model to predict axial buckling in knurled master rolls.

Question - I noticed around equation 3 or 4 that you had Poisson's ratio in there and it then dropped out. What happened?

Answer - This question refers to the out-of-plane solution. It is contained in the expression for flexural modulus, D.

Question - I have a feeling that it would contribute to instability if it was high value.

Answer - Observation of the expression for D in the paper indicates that a higher value of Poisson's ratio results in a lower value of D. A lower value of D means more propensity to axial buckling.

Question - Is your model only valid for center winding? And what changes if you have a surface winder?

Answer - The model presented today considers center winding with pressure roller assist. Key to the use of the model is a knowledge of the wound-in-tension. This is well known for center wind pressure roller assist winding. It is not clearly known for surface winding.

Question - Radial stability is driven by in-roll tension near the outside of the roll. Did you investigate taper tension to improve radial stability?

Answer - No, the winding tension profile in cases 2 and 3 was constant. The model can handle a general winding tension profile and therefore is able to study the problem you pose.

Question - Is the tension assumed to be constant in the Z direction (across the width)?

Answer - As stated in the presentation, winding tension can be user specified as a function of radius. At any radius, the in-roll stress model partitions the tension between

the independent axial segments by means of an outer lap force balance which accounts for the axially nonuniform radial profile. The effect of radial displacements is also included in the model. This capability was necessary to enable development of the model presented today.

Question - What is the tension level used in the experimental case?

Answer - Table 2, English units - 2 lbs tension 9 lbs nip force.